Appl. Phys. B 85, 101–104 (2006)
DOI: 10.1007/s00340-006-2350-7

Applied Physics B
Lasers and Optics

D. FAGUNDES-PETERS
A.S.S. DE CAMARGO✉
L.A.O. NUNES

Excited state absorption and energy transfer losses in thulium doped fluoroindogallate glass

Instituto de Física de São Carlos, Universidade de São Paulo – USP, Caixa Postal 369, CEP 13560-970, São Carlos – SP, Brazil

Received: 4 February 2006/Revised version: 7 May 2006
Published online: 1 July 2006 •

ABSTRACT Thulium doped fluoroindogallate glass was characterized by means of excited state absorption experiment in the 0.95 to 1.55 μm spectral range. The three bands corresponding to the electronic transitions $^3F_4 \rightarrow {}^3F_2$ (at 1.05 μm), $^3F_4 \rightarrow {}^3F_3$ (at 1.125 μm), and $^3F_4 \rightarrow {}^3H_4$ (at 1.45 μm) were observed. The energy transfer microscopic parameters for the reverse cross relaxation process $^3F_4$, $^3F_4 \rightarrow {}^3H_6$, $^3H_4$ were calculated for different multipolar interaction mechanisms using the Kushida model, and it was verified that the probability of this process is 100 times lower than that of the direct $^3H_4$, $^3H_6 \rightarrow {}^3F_4$, $^3F_4$ cross relaxation, responsible for the 1.8 μm emission pumping.

PACS 78.20.-e; 78.55.Qr; 42.70.Hj; 42.55.Wd

1 Introduction

The trivalent rare-earth ions with $4f^n$ configuration are the most used active ions for solid state lasers and optical amplifiers [1–8]. These ions can be conveniently pumped by low cost, high power diode lasers, to generate efficient emissions in the visible and near-infrared spectral regions. Particularly, the thulium emission at 1.8 μm ($^3F_4 \rightarrow {}^3H_6$ transition) has been largely studied in crystals and glasses, due to its important application in medicine. Since it matches a strong absorption band of water, it is used for the precise cut and ablation of biological tissues [9, 10]. The efficiency of such emission is highly dependent on energy transfer processes among Tm^{3+} ions. The $^3H_4$, $^3H_6 \rightarrow {}^3F_4$, $^3F_4$ cross relaxation (CR), for example, is the main pumping mechanism of the 1.8 μm emission resulting in the excitation of two ions in the emitting level $^3F_4$, while depopulating level $^3H_4$. The CR process is favored by the $^3H_4$, $^3H_6 \rightarrow {}^3H_6$, $^3H_4$ energy migration (EM), that spreads the excitation energy through the sample enabling more ions to interact. However, this spread energy can also be non-radiatively lost at structural defects. The reverse cross relaxation $^3F_4$, $^3F_4 \rightarrow {}^3H_4$, $^3H_6$, indicated by dashed lines in Fig. 1, constitutes a loss channel for the 1.8 μm emission, because it depopulates the emitting level $^3F_4$, while favoring emissions at 0.84 and 1.47 μm from level $^3H_4$.

In order to be appropriate for generation of 1.8 μm emissions, the host matrix for Tm^{3+} ions must present low phonon energies to minimize non-radiative decays. Among the vitreous compositions presenting such characteristic, chalcogenide and fluoride glasses are known as the most promising materials [8, 10]. Although chalcogenides present very low phonon energy ($\leq 400\,cm^{-1}$) that lead to high fluorescence quantum efficiency η, their structural and thermo-optical properties do not allow the use of high pump powers [11]. On the contrary, fluoride glasses associate high η with much better thermal and mechanical properties, making them interesting candidates for laser generation and amplification [12]. More specifically, the fluoroindogallate glass derived from the PGIZC composition [13], with low phonon energy ($520\,cm^{-1}$), and higher chemical stability than other fluoride compositions, is especially suitable for fiber am-

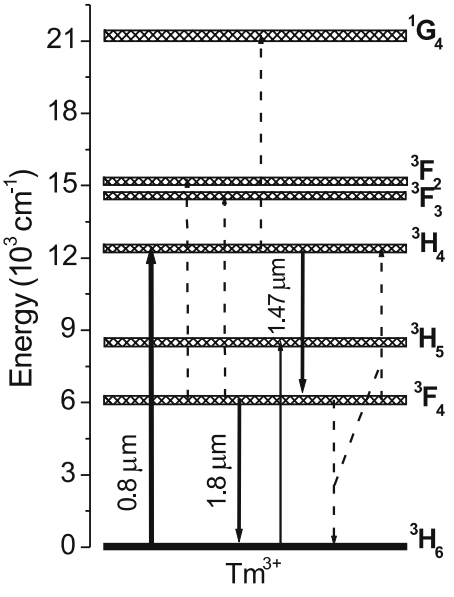

FIGURE 1 Schematic partial energy level diagram of Tm^{3+} in the fluoroindogallate glass host. The excitation, absorption and emission transitions are indicated by *solid lines*, and the ESA transitions and the reverse cross relaxation process are indicated by *dashed lines*

✉ Fax: +55 16 33739876, E-mail: andreasc@if.sc.usp.br

plifiers. Previous studies of radiative properties and energy transfer processes in Tm^{3+} doped PGIZC samples have indicated promising characteristics [14–16], but, in order to verify the feasibility of a 1.8 μm laser, a detailed study of the energy transfer losses in the near-infrared region was still required.

In this work, a pump–probe technique was used to measure excited state absorptions (ESA) in Tm^{3+} doped fluoroindogallate glass, in the 0.95 to 1.55 μm spectral range. The ESA data were used to calculate the energy transfer microscopic parameters, directly related to the probability of energy losses through the reverse cross relaxation $^3F_4$, $^3F_4 \rightarrow {}^3H_4$, $^3H_6$, by considering different multipolar interaction mechanisms.

2 Experimental

The studied set of Tm^{3+} doped fluoroindogallate glass samples was obtained as described in [14]. Their molar composition is: $30PbF_2$–$15InF_3$–$20GaF_3 - 15ZnF_2$–$(20-)CaF_2$–$XTmF_3$, with $X = 0.25, 0.5, 1.0, 1.5, 2.0, 3.0, 4.0$ and 6.0, hereafter named XTm. The refractive index of these samples for the sodium D line is 1.570. The luminescence spectra of the samples doped with 0.25 and 3.0% were measured with excitation at 680 nm, from a homemade dye (LDS 698) laser, pumped by a Nd:YAG laser at 532 nm. The signals were filtered by a 0.3 m monochromator and collected by an InAs detector. The same experimental setup was used for lifetime measurements of $^3F_4$, as a function of doping concentration, while the luminescence intensity decay was recorded by a digital oscilloscope Tektronix TDS 380.

The pump–probe experimental setup used for the ESA measurement of the 1.5% doped sample was that described in [17]. The pump source was a Ti:sapphire laser at 0.8 μm, modulated by a mechanical chopper at 14 Hz, and the probe light was provided by a tungsten lamp modulated at 600 Hz. The transmission of the probe beam by the pumped sample (ΔI) is different from that of the unpumped sample (I) because the absorption of the pump light causes a reduction in the ground state population. The ratio $\Delta I/I$ is related to the ground state absorption (GSA), stimulated emission (SE) and excited state absorption cross sections by:

$$\frac{\Delta I}{I} = n_e A L \left\{ \sigma_{GSA} + \sum_i \left(\frac{n_i}{n_e} \right) \left(\sigma_{SE,i} - \sigma_{ESA,i} \right) \right\} , \qquad (1)$$

where n_e is the overall excited population, A is the lock-in amplification factor, L is the sample length, n_i/n_e is the ratio of level i population and the total density of excited ions. The latter is directly proportional to the sum of lifetime values of the excited levels in the spectral region being considered (here, $^3H_4$ and $^3F_4$ of most relevance). Thus the ratio n_i/n_e can be obtained as the ratio of level i lifetime value and such sum of lifetime values. The ground and excited state absorption, and stimulated emission cross sections are described by σ_{GSA}, σ_{ESA} and σ_{SE}, respectively. The calibration of the $\Delta I/I$ spectra in cross section units was done in a spectral region where only ground state absorption and not stimulated emission or ESA were present. In this way the $n_e AL$ product could be obtained by equaling the $\Delta I/I$spectra with the σ_{GSA} spectra obtained using a Perkin Elmer Lambda 900 spectrophotometer.

3 Results and discussions

Figure 1 shows the partial energy level diagram of Tm^{3+} in the fluoroindogallate glass. The transitions corresponding to the excitation at 0.8 μm and to the emissions at 1.8 and 1.47 μm are indicated by the solid lines, and the ESA transitions from metastable levels $^3H_4$ and $^3F_4$, and the reverse cross relaxation energy transfer process, that can lead to upconversion, are indicated by dashed lines.

The luminescence spectra of a 0.25 mol % (solid line) and of a 3.0 mol % (dashed line) TmF_3 doped samples, obtained in the same arbitrary intensity scale, are presented in Fig. 2. The effect of energy transfer processes is clearly noticed by analyzing these spectra. It is observed that for the sample with lower doping concentration, in which ion–ion interactions are less probable due to higher interionic distance, the emissions at 0.84 and 1.47 μm, originating from the upper level $^3H_4$, present considerable intensity in comparison to the emission at 1.8 μm. However, when the doping concentration is increased, the CR and EM processes become highly probable, and while the emission at 1.8 μm shows an abrupt increase in intensity, those from $^3H_4$ are significantly diminished. These results are corroborated by the decrease in lifetime values of $^3H_4$ level with increasing concentration, for these same samples, as presented in [15]. Consequently, an appropriate choice of doping concentration is needed to optimize the efficiencies of 1.8 and 1.47 μm emissions. The reason why the 1.8 μm emission is also observed in the spectrum of the sample doped with 0.25 mol %, in which the CR is much less probable, lies in the excitation of $^3F_4$ through multiphonon decay from $^3H_4$.

Figure 3 presents the $\Delta I/I$ spectrum (solid line) of a 1.5 mol % TmF_3 doped sample calibrated in absolute cross section units. The results are very similar to those obtained for Tm^{3+} doped ZBLAN fluoride glass [12]. Given the short lifetime value of the $^3H_5$ level, stimulated emission or excited state absorptions are not expected from this level. Therefore, the band around 1.2 μm corresponds solely to the ground state

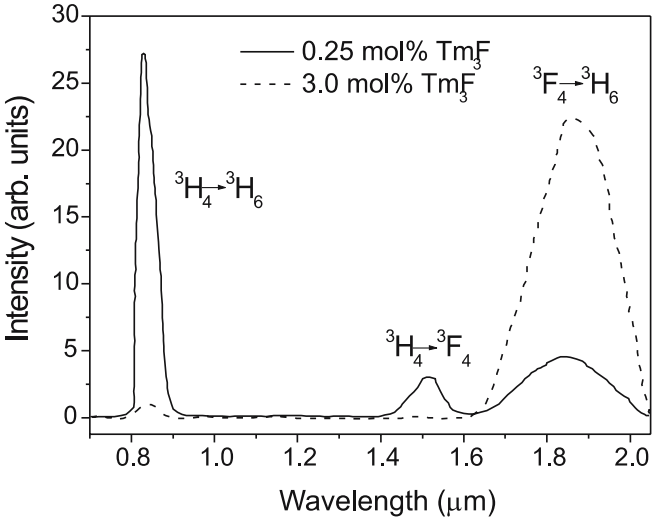

FIGURE 2 Luminescence spectra of fluoroindogallate glasses doped with 0.25 mol % (*solid line*) and 3.0 mol % TmF_3 (*dashed line*), under 0.68 μm diode laser excitation

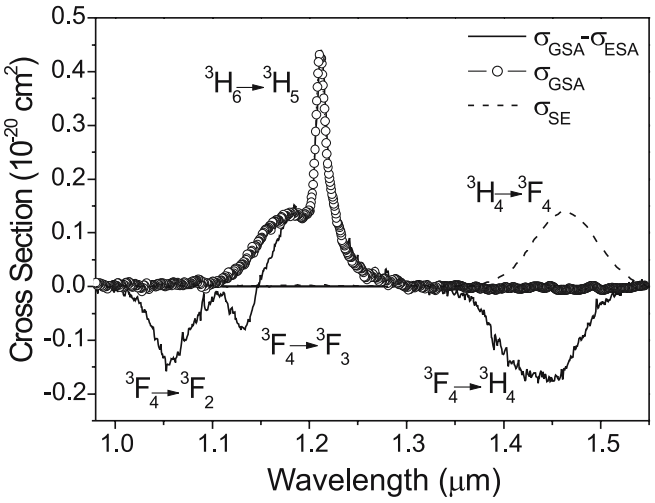

FIGURE 3 Ground state absorption (*open circles*) and $\sigma_{GSA} - 0.975\sigma_{ESA}$ (*solid line*) spectra measured for a 1.5 mol % TmF_3 doped fluoroindogallate glass. The *dashed line* corresponds to the emission cross sections for the $^3H_4 \rightarrow {}^3F_4$ transition, calculated using the Fuchtbauer–Ladenburg expression and the spontaneous emission spectrum

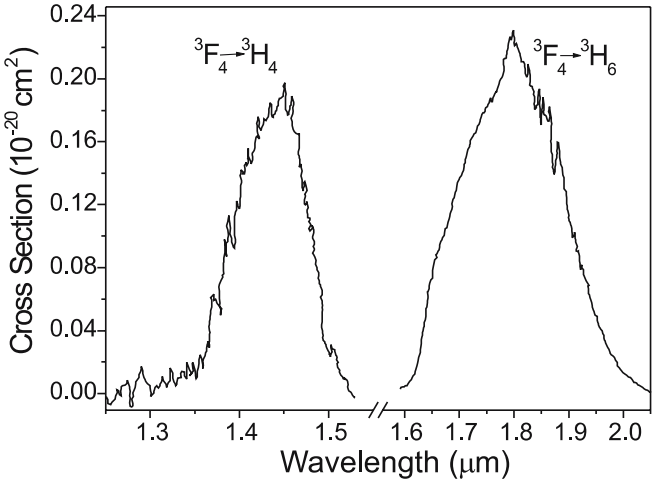

FIGURE 4 Acceptor ion absorption ($^3F_4 \rightarrow {}^3H_4$) and donor ion emission ($^3F_4 \rightarrow {}^3H_6$) cross section spectra. The cross section scale is common to both spectra and the emission spectrum was calibrated using the Fuchtbauer–Ladenburg expression [18]

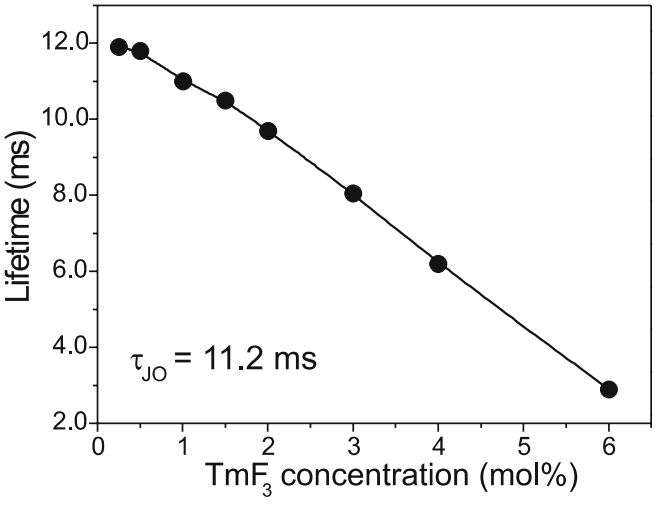

FIGURE 5 Dependence of lifetime values of $^3F_4$ level on TmF_3 doping concentration in the fluoroindogallate glass host

absorption $^3H_6 \rightarrow {}^3H_5$ and it was the one used to calibrate the $\Delta I/I$ spectrum by equaling it to the ground state absorption cross section spectrum obtained from an independent measurement (open circles). The $^3H_4 \rightarrow {}^3F_4$ stimulated emission spectrum (dashed line), also shown for comparison, was calculated from the spontaneous emission spectrum by using the Fuchtbauer–Ladenburg expression [18]. Three ESA bands are observed in Fig. 3: $^3F_4 \rightarrow {}^3F_2$ at 1.05 μm, $^3F_4 \rightarrow {}^3F_3$ at 1.125 μm, and $^3F_4 \rightarrow {}^3H_4$ at 1.44 μm. The lifetime value of $^3F_4$ level, for this 1.5% doped sample, is 10.5 ms and the relative population of this level, calculated as described in Sect. 2, is then $n_{^3F_4}/n_e = 0.975$. It is worth noting that the wavelength regions of $^3F_4 \rightarrow {}^3F_3$ and $^3H_4 \rightarrow {}^1G_4$ ESA transitions partially coincide. However, since the lifetime of the $^3F_4$ level is much longer than that of the $^3H_4$ level ($\tau = 270$ μs for the 1.5% doped sample), the pump source needs to be modulated at higher frequencies (around 100 Hz) in order to resolve the $^3H_4 \rightarrow {}^1G_4$ ESA transition. Such frequency resolved experiment was recently discussed by de Sousa et al. [19].

Although in the pump–probe experiment the stimulated emission, i.e., the amplification of the probe beam by the pumped sample can also be measured, according to (1), in the spectrum of Fig. 3 it is verified that the $^3H_4 \rightarrow {}^3F_4$ stimulated emission around 1.47 μm is not experimentally observed, due to the short lifetime value of $^3H_4$ level, as compared to $^3F_4$, which hinders population inversion, and due to the overlap of this emission with the intense $^3F_4 \rightarrow {}^3H_4$ ESA transition. If comparison is made between the calculated stimulated emission and the excited state absorption cross sections around 1.47 μm ($\sigma_{SE} = 0.15 \times 10^{-20}$ cm^2; $\sigma_{ESA} = 0.2 \times 10^{-20}$ cm^2), it can be inferred that optical gain cannot be achieved in Tm^{3+} doped fluoroindogallate glass under 0.8 μm excitation. On the other hand, it has been demonstrated that an alternative pumping scheme can be used to achieve amplification at this wavelength region [20–28].

By knowing the ESA cross section of the $^3F_4 \rightarrow {}^3H_4$ transition, it is possible to calculate the reverse cross relaxation microscopic parameters, using the Kushida model [29], for dipole–dipole, dipole–quadrupole and quadrupole-quadrupole interactions. Figure 4 presents the $^3F_4 \rightarrow {}^3H_6$ emission and

C_{d-a}^{dd} (cm^6/s)	C_{d-d}^{dd} (cm^6/s)	C_{d-a}^{dq+qd} (cm^8/s)	C_{d-d}^{dq+qd} (cm^8/s)	C_{d-a}^{qq} (cm^{10}/s)	C_{d-d}^{qq} (cm^{10}/s)
4.4×10^{-43}	29×10^{-40}	2.2×10^{-56}	8.5×10^{-53}	5.0×10^{-70}	3.6×10^{-66}

TABLE 1 Energy transfer microscopic parameters calculated by Kushida model for the donor–acceptor (d–a) $^3F_4$, $^3F_4 \rightarrow {}^3H_6$, $^3H_4$ reverse cross relaxation, and donor–donor (d–d) $^3F_4$, $^3H_6 \rightarrow {}^3H_6$, $^3F_4$ energy migration, in Tm^{3+} doped fluoroindogallate glass. The multipolar interactions are indicated by dd (dipole–dipole), dq (dipole–quadrupole) and qq (quadrupole–quadrupole)

the ${}^3F_4 \rightarrow {}^3H_4$ absorption bands. As can be seen, the two transitions are non resonant and in order to have spectral overlap between donor ion emission and acceptor ion absorption, the annihilation of three phonons of $520\,\mathrm{cm}^{-1}$ is necessary. The values of the microscopic parameters for the reverse cross relaxation calculated with the inclusion of the phonon annihilation as described in [16], as well as those for the ${}^3F_4$, ${}^3H_6 \rightarrow {}^3H_6$, ${}^3F_4$ energy migration [16], are presented in Table 1. Figure 5 presents the dependence of ${}^3F_4$ level lifetime values on Tm^{3+} concentration. The micro-parameters related to the reverse cross relaxation are two orders of magnitude smaller than those found for the ${}^3H_4$, ${}^3H_6 \rightarrow {}^3F_4$, ${}^3F_4$ direct cross relaxation [16]. From that, it is inferred that the quenching of level ${}^3F_4$ emission, as evidenced in Fig. 5, is mostly due to: (i) strong energy migration through ${}^3F_4$ level, followed by non-radiative transfer to structural defects; (ii) energy transfer to OH^- groups in the glass, with strong absorption at $1.8\,\mu\mathrm{m}$. These should be the main loss channels, rather than the reverse cross relaxation process. Still, optimized manufacturing procedures can minimize, to a good extent, the presence of OH^- and defects in the glass.

4 Conclusions

In conclusion, it was found that the microscopic parameters for the reverse cross relaxation is more than 100 times lower than those of the direct ${}^3H_4$, ${}^3H_6 \rightarrow {}^3F_4$, ${}^3F_4$ cross relaxation, indicating that the observed reduction in lifetime values of ${}^3F_4$ level, with increasing Tm^{3+} doping concentration, is mostly due to energy migration followed by non-radiative transfer to uncontrolled impurities in the samples. The fluoroindogallate glass is not appropriate for the construction of $1.47\,\mu\mathrm{m}$ Tm^{3+} fiber amplifiers pumped at $0.8\,\mu\mathrm{m}$, but efficient amplification might be achieved under another pumping scheme. This glass presents advantageous characteristics over the well known ZBLAN fluoride glass, such as higher chemical stability and larger thermal conductivity ($10.4 \times 10^{-3}\,\mathrm{WK}^{-1}\mathrm{cm}^{-1}$), better mechanical properties than chalcogenide glasses, and fairly high absorption and emission cross sections.

ACKNOWLEDGEMENTS This work was supported by the Brazilian funding agencies CNPq - Conselho Nacional de Desenvolvimento Científico e Tecnológico and FAPESP - Fundação de Amparo à Pesquisa do Estado de São Paulo.

REFERENCES

1 G. Fuxi, In *Laser Materials* (World Scientific, Singapore, 1995)
2 T Sakamoto, M. Shimizu, T. Kanamori, Y. Terunuma, Y. Ohishi, M. Yamada, S. Sudo, IEEE Photon. Technol. Lett. **7**, 983 (1995)
3 J. Kani, M. Jino, Electron. Lett. **35**, 1004 (1999)
4 A. Aozasa, T. Sakamoto, T. Kanamori, K. Hoshino, M. Shimizu, Electron. Lett. **36**, 418 (2000)
5 F. Roy, D. Bayart, A. Le Sauze, P. Baniel, IEEE Photon. Technol. Lett. **13**, 788 (2001)
6 T. Kasamatsu, Y. Yano, T. Ono, IEEE Photon. Technol. Lett. **13**, 433 (2001)
7 H. Chen, F. Babin, M. Leblanc, G. He, G.W. Schinn, J. Lightwave Technol. **21**, 1629 (2003)
8 S.S.-H. Yam, Y. Akasaka, Y. Kubota, H. Inoue, K. Parameswaran, IEEE Photon. Technol. Lett. **17**, 1001 (2005)
9 J.Y. Allain, M. Monerie, H. Poignant, Electron. Lett. **25**, 1660 (1989)
10 E.R.M. Taylor, L.N. Ng, J. Nilsson, R. Caponi, A. Pagano, M. Potenza, B. Sordo, IEEE Photon. Technol. Lett. **16**, 777 (2004)
11 S.M. Lima, J.A. Sampaio, T. Catunda, A.C. Bento, L.C.M. Miranda, M.L. Baesso, J. Non-Cryst. Solids **273**, 215 (2000)
12 S. Guy, A.M. Jurdyc, B. Jacquier, W.M. Meffre, Opt. Commun. **250**, 344 (2005)
13 G. Zhang, B. Friot, M. Poullain, J. Non-Cryst. Solids **213,214**, 6 (1997)
14 K. Miazato, D.F. de Sousa, A. Delben, J.R. Delben, S.L. de Oliveira, L.A.O. Nunes, J. Non-Cryst. Solids **273**, 246 (2000)
15 D.F. de Sousa, R. Lebullenger, A.C. Hernandes, L.A.O. Nunes, Phys. Rev. B **65**, 094 204 (2002)
16 D.F. de Sousa, L.A.O. Nunes, Phys. Rev. B **66**, 024 207 (2002)
17 J. Koetke, G. Huber, Appl. Phys. B **61**, 151 (1995)
18 W.J. Miniscalco, R.S. Quimby, Opt. Lett. **16**, 258 (1991)
19 D.F. de Sousa, V. Peters, G. Huber, A. Toncelli, D. Parisi, M. Tonelli, Appl. Phys. B **77**, 817 (2003)
20 T. Komukai, T. Yamamoto, T. Sugawa, T. Miiyajima, Electron. Lett. **29**, 110 (1993)
21 Y. Miyajima, T. Komukai, T. Sugawa, Electron. Lett. **29**, 660 (1993)
22 R.M. Percival, D. Szebesta, S.T. Davey, Electron. Lett. **28**, 1866 (1992)
23 R.M. Percival, D. Szebesta, S.T. Davey, Electron. Lett. **29**, 1054 (1993)
24 T. Komukai, T. Yamamoto, T. Sugawa, T. Miiyajima, IEEE J. Quantum Electron. **QE-31**, 1880 (1995)
25 C. Barnard, P. Myslinski, J. Chrostowski, M. Kavehrad, IEEE J. Quantum Electron. **QE-30**, 1817 (1994)
26 T. Schweizer, P.E.-A. Möbert, J.R. Hector, D.W. Hewak, W.S. Brocklesby, D.N. Payne, G. Huber, Phys. Rev. Lett. **80**, 1537 (1998)
27 S. Kishimoto, K. Hirao, J. Non-Cryst. Solids **213,214**, 393 (1997)
28 N. Garnier, R. Moncorgé, H. Manaa, E. Descroix, P. Laporte, Y. Guyot, J. Appl. Phys. **79**, 4323 (1996)
29 T. Kushida, J. Phys. Soc. Jpn. **34**, 1318 (1973)